Table 1 Function and gradient calls required for convergence

Problem number	NG	Analytical gradient NF	Analytical gradient NEF	Discrete gradient NF
1	39	122	317	317
2	32	105	201	201
3	44	133	353	387
4	70	209	489	506
5	35	105	175	177
6[a]	26	92	144	144
7	18	55	109	109
8	10	24	44	44
9[b]		(not run)		335
10		(not run)		111

[a]Reciprocals of x and x_2 occur in problem 6, and the maximum of the objective function can be made arbitrarily large by assigning $x_1 = \epsilon$ and $x_2 = -\epsilon^2$ with $0 < \epsilon << 1$. To avoid this, weight w_2 was held at 100 and w_3 at 1000, and the lower bounds on both x_1 and x_2 were increased from 0 to 0.1.

[b]The solution to problem 9 terminated before gradient convergence criteria were satisfied, but accuracy in the final value of f was within 6 significant figures of the optimum.

Table 2 Normalized CPU times for convergence

Problem number	Analytical gradient	Discrete gradient
1	0.0410	0.0471
2	0.0243	0.0248
3	0.0335	0.0370
4	0.0304	0.0339
5	0.0201	0.0211
6	0.0203	0.0222
7	0.0220	0.0217
8	0.0166	0.0168
9	(not run)	0.6921
10	(not run)	0.2532

units. And finally, when an executable load module for the problem was prepared so that execution in the short calling program terminated without calling LPNLP to solve the problem, the loading and execution of this required 0.0076 units. If a given problem is of large dimension or is to be run with many different data sets (different constraint bounds perhaps) the normalized times for each execution, such as given in Table 2, are important. However, if a low dimensioned problem is to be solved but once, the time required to link the optimization code is often more significant.

The performance of LPNLP is dependent on scaling of variables and constraint functions. Except for problem 7, however, the scale factors given in Refs. 1 and 2 were used. For problem 7, the constraints as given[1] are

$$x_1^2 x_2 \leq 675.0 \tag{5}$$

and

$$10^{-7}(x_1 x_3)^3 \leq 0.419 \tag{6}$$

A common weighting factor is used for both of these constraints in LPNLP. In order to have these constraints weighted more evenly, they were scaled as follows:

$$0.1 x_1^2 x_2 \leq 67.5 \tag{7}$$

and

$$10^{-5}(x_1 x_3)^3 \leq 41.9 \tag{8}$$

with which results were obtained as given in Tables 1 and 2.

Conclusion

LPNLP is a robust optimization code; in addition to the low dimensioned problems of this work, it has been applied with success[7,8] to problems having as many as 20 variables and numerous constraints, and to a 100 variable generalization of problem 5. The development of augmented Lagrangian methods should do much to offset previously reported dissatisfaction[1,3] with gradient-based methods. Also, the Lagrange multipliers, which are obtained as an integral part of each solution, are a valuable adjunct to solution sensitivity analysis.[7] The documentation and FORTRAN program listings for LPNLP are readily available. Information on how to obtain card source can be obtained from the author.

References

[1]Eason, E.D. and Fenton, R.G., "A Comparison of Numerical Optimization Methods for Engineering Design," *Transactions of the ASME, Ser. B: Journal of Engineering for Industry*, Vol. 96, Feb. 1974, pp. 196-200.

[2]Eason, E.D. and Fenton, R.G., "Testing and Evaluation of Numerical Methods for Design Optimization," Rept. UTME-TP 7204, Sept. 1972, Dept. of Mechanical Engineering, Univ. of Toronto, Toronto, Canada, Sept. 1972.

[3]Pappas, M., "Performance of the 'Direct Search Design Algorithm' as a Numerical Optimization Method," *AIAA Journal*, Vol. 13, June 1975, pp. 827-829.

[4]Hestenes, M.R., "Multiplier and Gradient Methods," *Journal of Optimization Theory and Applications*, Vol. 4, Nov. 1969, pp. 303-320.

[5]Powell, M.J.D., "A Method for Nonlinear Constraints in Minimization Problems," in *Optimization*, R. Fletcher (editor), Academic Press, New York, 1969.

[6]Pierre, D.A., "Multiplier Algorithms for Nonlinear Programming," *Presented at the 8th International Symposium on Mathematical Programming*, Aug. 1973.

[7]Pierre, D.A. and Lowe, M.J., *Mathematical Programming Via Augmented Lagrangians: An Introduction with Computer Programs*, Addison-Wesley, Reading, Mass. 1975.

[8]Pierre, D.A. and Dudding, C.H., "Constrained Optimization with Gradient Approximations," *IEEE Transactions on Systems, Man, and Cybernetics*, Vol. SMC-7, Feb. 1977.

[9]Colville, A.R., "A Comparative Study on Nonlinear Programming Codes," IBM New York Scientific Center Report No. 320-2949, June 1968.

Static Pressure in Hypersonic Nozzle Boundary Layers

P. J. Finley*
Imperial College of Science and Technology, London, England

LARGE variations of static pressure may be observed in hypersonic boundary-layer flows (see Kemp and Owen,[1] Fig. 9, for a collection of observations), and are shown below to result from the combined effects of longitudinal curvature of the mean streamlines and the increasing importance, as the Mach number rises, of the Reynolds stress contribution to the total normal stress perpendicular to the wall.

The momentum equation normal to a streamline may be written

$$(\partial\sigma/\partial n) = (\partial/\partial n)(\bar{p} + \bar{\rho}\overline{v'^2}) = -\rho U^2/R_x \tag{1}$$

where σ is the total normal stress made up of contributions from the mean static pressure $\bar{p}$ and the mean normal Reynolds stress $\bar{\rho}\,\overline{v'^2}$, and R_x, the longitudinal radius of curvature of the streamline, is defined positive for concave walls. In hypersonic flows the specific momentum flux ρU^2 is potentially very large compared with the mean static pressure $\bar{p}$, and if therefore we integrate Eq. (1) across a boundary

Received Jan. 17, 1977; revision received March 8, 1977.
Index categories: Boundary Layers and Convective Heat Transfer—Turbulent; Supersonic and Hypersonic Flow.

*Lecturer, Department of Aeronautics.

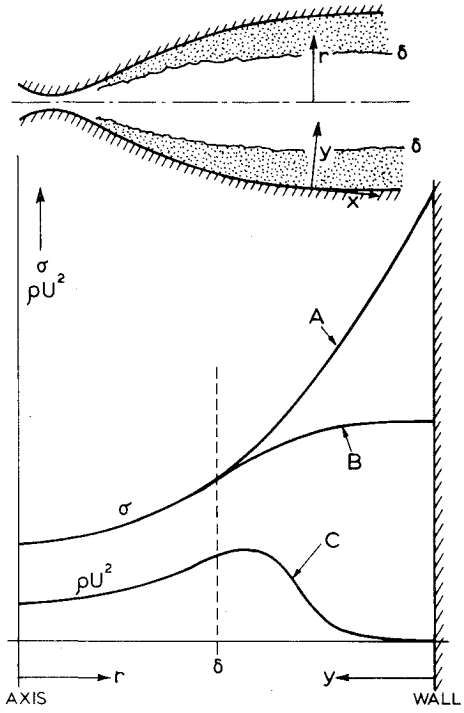

Fig. 1 Variation of normal stress σ in a contoured hypersonic nozzle. Curve A: normal stress σ as it would be determined for inviscid flow by a characteristic calculation starting from the pressure distribution on the axis. Curve B: normal stress distribution as modified by the existence of the boundary layer. Curve C: specific momentum flux distribution showing the fall which occurs in the boundary layer.

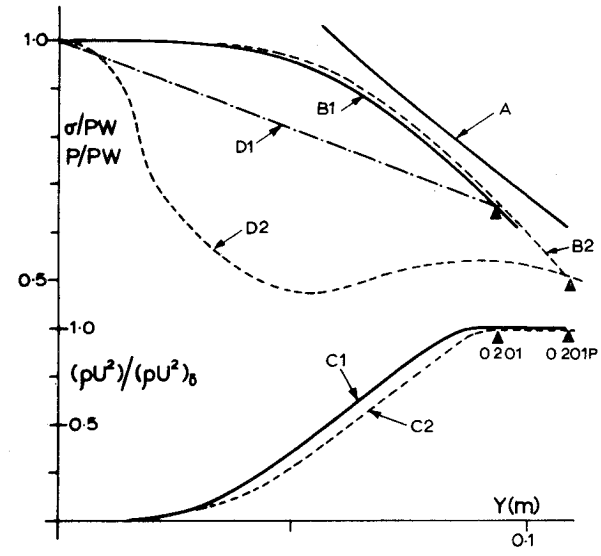

Fig. 2 Normal stress and static pressure observed in an M20 nozzle (Beckwith et al.)[2] Curve A: σ/PW for inviscid flow as calculated by the authors. Curves B1 and B2: σ/PW as modified by the boundary layer. Calculated according to App. 1 for the data as presented assuming a linear pressure distribution (0201, B1), and using the authors' measured static pressure distribution (0201P, B2). See curves D1 and 2. Cuves C1 and C2: specific moment flux distribution for 0201(C1) and 0201P(C2). Curves D1 and D2: static pressure distribution as assumed by the authors in data reduction (0201,D1) and as obtained from corrected static pressure probe measurements (0201P,D2). ▲ = assumed boundary-layer edge points.

layer of width δ, we see that the proportional change in normal stress due to mean flow curvature

$$(\Delta\sigma/\sigma) = |0|\gamma M_\infty^2 (\delta/R_x) \tag{2}$$

may well be large for quite modest values of δ/R_x.

The variation of σ in a contoured nozzle wall boundary layer is sketched in Fig. 1. (In this figure and in all the discussion below second-order effects such as those arising from the slightly differing directions of the "r" and the "y" axes are neglected.) Curve A shows a typical variation of normal stress as it might be calculated for inviscid flow from a given centerline Mach number distribution. The slope steadily increases as the wall is approached, as a consequence of the steady increase in streamline curvature, reinforced by the increase in density which accompanies the increase in pressure. The existence of the boundary layer modifies this to a curve of the type shown as B, meeting the wall at right angles. The gradient of σ falls as the specific momentum flux falls in the boundary layer. At hypersonic Mach numbers, this change is almost entirely due to the falling density—in the cases discussed below the density has fallen to 0.1-0.4 of the freestream value before the velocity has fallen by 10%.

As implied by Eq. (1) the static pressure $\bar{p}$ and the normal stress σ may well differ significantly. At very high Mach numbers, although $\overline{v'^2}$ is small when compared to U^2, $\bar{\rho}\,\overline{v'^2}$ may still be of the same order as $\bar{p}$. If the various Reynolds stresses are assumed to be of the same order, then we may write

$$\bar{\rho}\overline{v'^2} = |0|\tau_w = |0|\gamma p_\infty M_\infty^2 c_f \tag{3}$$

This is almost certainly a gross oversimplification, but does allow an estimate of the likely magnitude of the Reynolds stress and an explanation of some puzzling features of the reported observations.

There are two hypersonic nozzle wall experiments for which a static pressure profile is reported. If Reynolds stresses are of the same order as the static pressure it is far from certain that a static pressure probe actually records the static pressure, but the data are accepted here as they stand.

Beckwith et al.[2] made a functionally complete set of profile measurements in a cooled-wall M20 nozzle (7105 0201P) and this is supported by a wall shear stress measurement (Harvey and Clark[3]) under closely matched conditions. A feature of the experiment was the very large amount of correction needed in reducing the data (calibration procedures caused readings to be changed by as much as a factor of 2) so that no very great reliance should be placed on any precise numerical values. Figure 2 shows their results together with a determination of σ as described in the Appendix. Values are shown using both the measured static pressure (0201P) and a linear pressure variation used by the authors in data reduction (0201). If Eq. (3) is written

$$\Delta\bar{p}(\max) = (\sigma - \bar{p})\,(\max) = (\overline{\rho v'^2})\,(\max) = K\gamma p_\infty M_\infty^2 c_f \tag{4}$$

these observations give the value of K as 2.77.

Fischer et al.[4] studied a near-adiabatic M22 nozzle boundary layer, and Fig. 3 shows the variation of $\bar{p}$ and σ for the one set (7001 0104) for which they made functionally complete profile measurements. They replaced the measured static pressure distribution by the set of straight lines shown here (the original data are shown in Figs. 13 and 14 of the source paper) and the general shape is not dissimilar to that shown in Fig. 4. They did not measure wall shear stress, but give an estimate obtained from the limiting slope of the velocity profile. Using this value, K [Eq. (4)] is found as 3.7.

The static pressure profile is thus determined by the normal stress-momentum equation (1), the pressure differing from the normal stress by an amount of up to $\Delta\bar{p}$ as given by Eq. (4). It is suggested, as a working hypothesis, that K be set at 3, giving a slight preference to the Beckwith et al. value as it is based on a measured wall stress. There remain several inconsistencies in the determination of K, but any resulting inaccuracy is unlikely to exceed the marked uncertainty of the data. Unfortunately $\Delta\bar{p}$(max) will only be significant in comparison with $\bar{p}$ at very high Mach numbers, when the

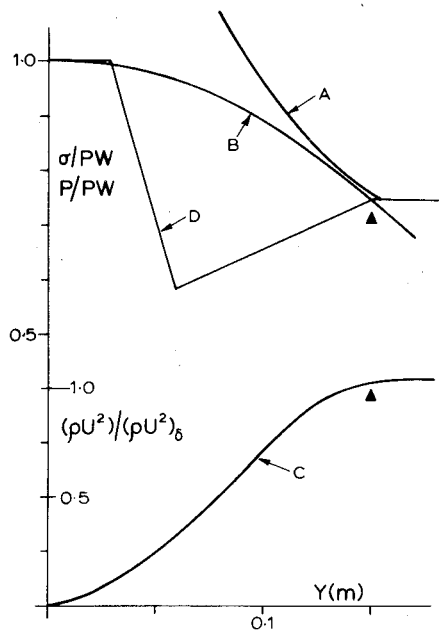

Fig. 3 Normal stress and static pressure observed in an M22 nozzle (Fischer et al.).[4] Curve A: σ/PW for inviscid flow (D. M. Bushnell).[10] Curve B: σ/PW as modified by the boundary layer, calculated as in App. 1. Curve C: specific moment flux distribution. Curve D: author's representation of static pressure as measured with a static probe, and used in data reduction. ▲ = assumed boundary-layer edge point.

measurement of $\bar{p}$ is so difficult that it is better to describe a measurement as an estimate. Further difficulties arise as the freestream random disturbance level in hypersonic facilities is high, and $\bar{\rho}\overline{v'^2}$ in the freestream may well be comparable with, even if smaller than, $\bar{\rho}\,\overline{v'^2}$ in the most intensely turbulent part of the boundary layer (see Kemp and Owen,[1] Fig. 28b), so that the static pressure would then be below the total normal stress. These disturbances are not necessarily "turbulent" but may originate as pressure waves propagated by the turbulent nozzle wall boundary layer upstream of and on the opposite side to the test station (Stainback and Anders).[5]

The collection by Kemp and Owen,[1] cited above, of static pressure differences across a boundary layer can now be seen to attempt to correlate, on a single basis, two distinct phenomena. There is the large and easily explained pressure difference (a function not only of M but also of radius of curvature) required to provide a centripetal acceleration in flows with curved mean flow streamlines, and there is the lesser, but at high Mach numbers significant, effect resulting from the normal stress contribution of the Reynolds stress. Further work is required, however, to explain some of the differences reported for straight-wall flow, and especially the recent data of Laderman and Demetriades[6] and Backx.[7] A preliminary discussion of some of the factors involved may be found in Fernholz and Finley.[8]

The results of Beckwith et al,[2] if taken at their surface value, indicate that at its peak value the Reynolds stress may provide a normal stress contribution equal to that of the mean static pressure. If boundary-layer data are to have any general application, it must be possible to provide a basis for comparison between different experiments. Perhaps the most useful, and certainly the most commonly used, parameters employed are the Reynolds numbers based on momentum defect thickness. In the Mach number range of this experiment the velocities vary very little over the Y-range contributing most to the integrand of momentum thickness, which will therefore be modified almost directly by the value of the density assumed. The selection of one of curves B (total normal stress), D1 (linear static pressure variation), or D2 (measured static pressure variation), in Fig. 2, rather than another could lead to a large difference in the calculated value of Θ. The distinction here is unfortunately confused by the differing values of freestream static pressure, which cannot be reconciled both with each other and with the reported tunnel reservoir pressure. The analysis above does, however, make it possible to estimate the magnitude of the Reynolds stress contribution, and, to the extent that it is possible to accept these very difficult static pressure measurements, to make a first attempt at scaling the distribution of $\Delta\bar{p}$ through the boundary layer. The resulting mean static pressure distribution should be noticeably more accurate than the linear variation generally assumed by authors to date.

Appendix: Calculation of the Total Normal Stress Distribution

The distribution $\sigma(y)$ is in principle calculated from Eq. (1) as

$$\sigma(y) = \sigma(y=0) - \int_0^y (\rho u^2/R_x)\,dy$$

The values of $\bar{\rho}$, $\bar{u}$ were taken from the authors' original profile tabulations as edited by Fernholz and Finley.[9] The data in question were obtained by Fischer et al.[4] (serial 7001 0104) and Beckwith et al.[2] (serials 7105 0201/0201P).

Values of the local streamline curvature are not available, and the integration was performed assuming that the y-range was sufficiently small for R_x to be treated as constant. The resulting normal stress variation was then scaled to fit the wall static pressure and the static pressure at the boundary-layer edge point.

There are various inconsistencies in the data shown in Fig. 2. These arise from the fact that the static pressure near the boundary-layer edge can be assigned three values, derived from a characteristic calculation based on measurements made on the centerline, shown as curve A, obtained from the pitot measurements and the tunnel reservoir pressure (used for 0201), or taken from the much corrected static pressure measurements (used for 0201P). A full discussion is given in connection with Fig. 7 of the source paper.[2]

Acknowledgment

This work was performed in connection with the preparation of the data catalog of Ref. 9 and was funded by the German Science Research Council (DFG) and the Technical University, Berlin. The author wishes to acknowledge many helpful conversations with P. Bradshaw, D. M. Bushnell, and H. H. Fernholz.

References

[1]Kemp, J. H. and Owen, F. K., "Experimental Study of Nozzle Wall Boundary Layers at Mach Numbers 20 to 47," NASA TN D-6965, 1972.

[2]Beckwith, I. E., Harvey, W. D., and Clark, F. L., "Comparisons of Turbulent Boundary Layer Measurements at Mach Number 19.5 with Theory and an Assessment of Probe Errors," NASA TN D-6192, 1971.

[3]Harvey, W. D. and Clark, F. L., "Measurement of Skin Friction on the Wall of a Hypersonic Nozzle," *AIAA Journal*, Vol. 10, Sept. 1972, pp. 1256-1258.

[4]Fischer, M. C., Maddalon, D. V., Weinstein, L. M., and Wagner, R. D., "Boundary-Layer Surveys on a Nozzle Wall at $M=20$, Including Hot-Wire Fluctuation Measurements," *AIAA Journal*, Vol. 9, May 1971, pp. 826-834.

[5]Stainback, P. C. and Anders, J. B., "Disturbance Measurements in a Mach 5 Wind Tunnel," Pt. I, AIAA Paper 74-136, Washington, D.C., 1974.

[6]Laderman, A. J. and Demetriades, A., "Mean and Fluctuating Flow Measurements in the Hypersonic Boundary Layer over a Cooled Wall," *Journal of Fluid Mechanics*, Vol. 63, 1974, pp. 121-144.

[7]Backx, E., "A Study of the Turbulent Boundary Layer at $M=15$ and 19.8 on the Wall of a Conical Nozzle," PhD Thesis; VKI/Catholic University, Louvain, 1975.

[8]Fernholz, H. H. and Finley, P. J., "A Critical Compilation of Compressible Turbulent Boundary Layer Data," VKI Lecture Series 86, "Compressible Turbulent Boundary Layers," March 1976.
[9]Fernholz, H. H. and Finley, P. J., "A Critical Compilation of Compressible Turbulent Boundary Layer Data—Data Compilation," AGARD-AG-223. To be published in 1977.
[10]Bushnell, D. M., Private communication.

An Edge-Corrected Linearization Technique for Boundary-Layer Problems

Richard S. Hirsh*
McDonnell Douglas Corporation, Long Beach, Calif.

FOR parabolic marching problems, as exemplified by boundary-layer calculations, implicit finite-difference procedures are preferable to explicit ones due to the lack of a stability restriction on the size of the marching step. The penalty paid for this theoretically unlimited step size is the need to solve a nonlinear set of equations at each step. This can be overcome by an efficient iteration scheme,[1] or any number of linearization techniques; see for example, the methods used in Refs. 2-4. Probably the most common linearization used is a simple quadratic extrapolation from previously calculated points, which is accomplished by a direct Taylor expansion about the desired point. This Note will show that this extrapolation procedure introduces errors into the computed solution if the imposed boundary conditions vary with the marching variable. A simple and effective alteration to the usual procedure, called edge-corrected linearization (ECL), is introduced to alleviate the difficulty.

If, during a marching procedure, we wish to advance from a point (i) to a point $(i+1)$, and center the differencing about the point $(i+\frac{1}{2})$, i.e., a Crank-Nicolson type second-order-accurate integration, the extrapolated nonlinear coefficients (denoted by capitals) may be expressed for a given j as

$$U=u_{i+\frac{1}{2}}=\frac{3}{2}u_i-\frac{1}{2}u_{i-1}+\frac{3}{2}(\Delta x)^2u''_{i+\frac{1}{2}} \tag{1a}$$

if the function values are stored at points (i), $(i-1)$, etc., and

$$W=w_{i+\frac{1}{2}}=2w_{i-\frac{1}{2}}-w_{i-3/2}+4(\Delta x)^2w''_{i+\frac{1}{2}} \tag{1b}$$

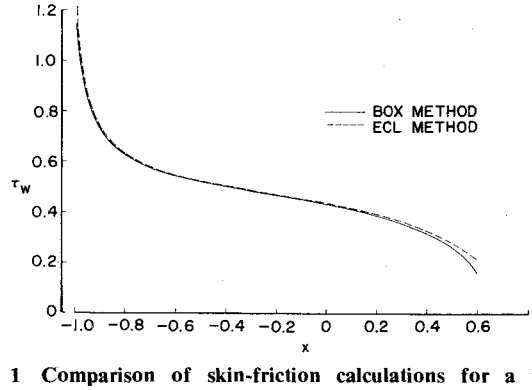

Fig. 1 Comparison of skin-friction calculations for a prolate spheroid at 0° incidence.

Received Jan. 24, 1977; revision received March 22, 1977.
Index categories: Computational Methods; Boundary Layers and Convective Heat Transfer—Laminar and Turbulent.
*Senior Engineer/Scientist.

if the values are stored at the midpoints, where Δx is the step size. An example of the use of this formulation in a standard boundary-layer calculation is given below.

The boundary-layer equations for incompressible flow past an arbitrary body of revolution are

$$(1/h)uu_x+wu_z=-(1/h)p_x+u_{zz} \tag{2}$$

$$(1/h)u_x+K_{2/}u+w_z=0 \tag{3}$$

where the Reynolds number has been scaled into z and w. To integrate these equations, Eq. (2) is cast in difference form centered at a mid-step point, $(i+\frac{1}{2})$, with any nonlinear values evaluated by relations (1). That is

$$\frac{1}{h_{i+\frac{1}{2}}}U\left(\frac{u_{i+1,j}-u_{i,j}}{\Delta x}\right)+W\left[\frac{1}{2}(\delta_zu_{i,j}+\delta_zu_{i+1,j})\right]$$

$$=-\frac{1}{h_{i+\frac{1}{2}}}p_{x_{i+\frac{1}{2}}}+\left[\frac{1}{2}(\delta_z^2u_{i,j}+\delta_z^2u_{i+1,j})\right] \tag{4}$$

where δ_z and δ_z^2 are the standard centered difference operators. The differencing represented by Eq. (4) yields a tridiagonal system for the unknowns $u_{i+1,j}$ which can be easily solved. Once this is done, the continuity equation, (3), can be written for w at the midpoint $(i+\frac{1}{2})$ and integrated out from the wall to get the new values of $w_{i+\frac{1}{2},j}$.

This fairly standard approach to the solution of simple boundary-layer problems can lead to spurious effects when the values of the velocity in Eqs. (2) and (3) are not normalized by their edge values (and hence equal to unity at each marching step), but allowed to vary with x. These effects can be traced directly to the extrapolation scheme, Eqs. (1). Consider Eq. (2) at the edge of the boundary layer and beyond. Here, the z gradients are negligible. The pressure gradient is, as usual, known from the edge conditions. Thus, the difference form of Eq. (2) in this region of the boundary layer, where $j=J$ is

$$\frac{1}{h_{i+\frac{1}{2}}}U\left(\frac{u_{i+1,J}-u_{i,J}}{\Delta x}\right)=-\frac{1}{h_{i+\frac{1}{2}}}p_{x_{i+\frac{1}{2}}}$$

$$=\frac{1}{h_{i+\frac{1}{2}}}(u_eu_{ex})_{i+\frac{1}{2}}$$

Evaluating the edge velocity and its gradient at $(i+\frac{1}{2})$

$$U(u_{i+1,J}-u_{i,J})=\left(\frac{u_{e_i}+u_{e_{i+1}}}{2}\right)(u_{e_{i+1}}-u_{e_i})$$

which gives, for the unknown velocity $u_{i+1,J}$

$$u_{i+1,J}=\left\{\frac{[(u_{e_i}+u_{e_{i+1}})/2]}{U}\right\}(u_{e_{i+1}}-u_{e_i})+u_{i,J} \tag{5}$$

where $u_{i,J}=u_{e_i}$ if we assume that we are advancing away from a station with a correct velocity profile. Thus, if the extrapolated value, U, is not equal to the correct midpoint value, $[(u_{e_i}+u_{e_{i+1}})/2]$, the computed value at the point J will be in error. The more severe the pressure gradient, i.e. the stronger the variation of u_e, the more the calculated value will deviate from the true value.

Calculations were performed for the boundary layer on a prolate spheroid of thickness ratio 1/4. The manifestation of the extrapolation error is evident in a lack of exponential decay of the u-velocity within the boundary layer to its edge value. With a value of the last z-station larger than the boundary-layer thickness, a calculation using the box method with Newton iteration reproduced the freestream velocity exactly. The Crank-Nicolson integration with extrapolation